Poroelasticity Benchmarking for FEM on Analytical Solutions

E. Holzbecher
Georg-August Universität Göttingen
GZG Applied Geology, Goldschmidtstr. 3, 37077 Göttingen, GERMANY; E-mail: eholzbe@gwdg.de

Abstract: We examine the poroelastics mode, which couples hydraulics and mechanics by some basic benchmarks. For cases with analytical solutions we check the accuracy for changing meshes and calculate the convergence rate.

Keywords: Poroelastics, porous media flow, cavity problem, analytical solution, convergence rate

1. Introduction

In poroelastics hydraulic and mechanical processes are coupled, which allows the simultaneous modeling of these processes (HM-coupling) in porous media. Applications for this type of modeling are generally necessary in all situations, in which flow processes through a porous material are accompanied by deformations. The pore pressure as a variable is responsible for fluid flow and movements of the solid, and also depends on both fluid and solid states.

There are several fields of applications, in which poroelastical modeling, as described, is relevant. In geological systems high flow velocities may lead to changes of the solid material, as in the vicinity of pumping or injecting wells. Concerning the exploitation of oil and gas reservoirs poroelasticity may become crucial. The technique of hydraulic fracking utilizes the mentioned coupling. Problems of land subsidence are often related to changes in the subsurface flow system. Aside from soil and rocks the coupling of hydraulic and mechanical features becomes relevant in artificial materials, for example for hydro gels and for swelling, highly pronounced in sponges. Tissue mechanics is a branch of material sciences concerned with such substances (Cowin & Doty 2007).

The model considers Darcy-flow within porous medium and elastic behaviour of the solid material. We compute deformation and pore pressures within the entire domain. The coupling with poroelasticity is achieved using an additional source term in the fluid mass conservation equation.

2. Mathematical description

The mechanical model is given by the equations

$$\begin{aligned} &-\nabla\cdot\boldsymbol{\sigma}=\mathbf{F}_V,\boldsymbol{\sigma}=\mathbf{s}\\ &\mathbf{s}-\mathbf{s}_0=\mathbf{C}:\left(\boldsymbol{\varepsilon}-\boldsymbol{\varepsilon}_0-\boldsymbol{\varepsilon}_{inel}\right)-\alpha p\mathbf{I}\\ &\boldsymbol{\varepsilon}=\tfrac{1}{2}\left(\left(\nabla\mathbf{u}\right)^T+\nabla\mathbf{u}\right)\\ &\rho S\frac{\partial p}{\partial t}+\nabla\cdot\left(\rho\mathbf{q}\right)=Q-\rho\alpha\frac{\partial\varepsilon_V}{\partial t}\\ &\mathbf{q}=-\frac{k}{\mu}\nabla p \end{aligned} \qquad (1)$$

with stress tensors $\boldsymbol{\sigma}$ and $\mathbf{s}$, volume force vector $\mathbf{F}_V$, strain tensor $\boldsymbol{\varepsilon}$, deformation vector $\mathbf{u}$, pore pressure p, elastic tensor $\mathbf{C}$ and Biot constant α. Subscript 0 denotes initial values, and *inel* indicates the inelastic part of the strain.

For zero initial stress and strain, elastic material and gravity as only force the mechanical model reduces to:

$$\begin{aligned} &-\nabla\cdot\boldsymbol{\sigma}=\left(\rho\theta+\rho_b\right)\mathbf{g}\\ &\boldsymbol{\sigma}=\mathbf{C}\cdot\boldsymbol{\varepsilon}-\alpha p\mathbf{I}\\ &\boldsymbol{\varepsilon}=\tfrac{1}{2}\left(\left(\nabla\mathbf{u}\right)^T+\nabla\mathbf{u}\right) \end{aligned} \qquad (2)$$

with porosity θ, fluid density ρ and bulk density ρ_b.

In the model mechanical and hydraulic processes are coupled with each other. The hydraulic model is described by:

$$\begin{aligned} &\rho S\frac{\partial p}{\partial t}+\nabla\cdot\left(\rho\mathbf{q}\right)=Q-\rho\alpha\frac{\partial\varepsilon_V}{\partial t}\\ &\mathbf{q}=-\frac{k}{\mu}\nabla p \end{aligned} \qquad (3)$$

with Darcy velocity $\mathbf{q}$, permeability k, fluid dynamic viscosity μ, storage parameter S, fluid source/sink-term Q, volumetric strain ε_V.

The Biot coefficient appears in the stress-strain relation (second equation of systems (1) and (2)) as a weighting factor for the influence of fluid pressure. Moreover α appears as coefficient in an additional storage term in the

flow equation (first equation of system (3)). For the steady state the coupling is only one-way, as the time derivatives in the flow equation vanish. For the transient case the coupling between the mechanical and the hydraulic is two-way: the fluid pressure influences the stress-strain relation and thus the deformations. Vice versa the flow equation is changed via the volumetric strain. In general both models have to be performed simultaneously in order to take the mutual effects between mechanics and hydraulic into account.

The analytical approach with parameter α was introduced by M.A. Biot already in the first half of the last century (Biot, 1941) and is used until today with only minor modifications (for example: Morency *et al.,* 2007). Carcione *et al.* (2010) present a review on the relevance of Biot's theory in computational poroelasticity.

3. Numerical Model Set-up

The mathematical finite element code COMSOL Multiphysics (2012) for the solution a systems of partial differential equations is suited for a big variety of couplings of different physical phenomena. Here we focus on the interaction between hydraulics and mechanics. However, to extend the models to account for thermal processes within that software environment is a straight-forward task and will be reported elsewhere. COMSOL Multiphysics allows easy operation via a graphical user interface. Several toolboxes allow the specific set-up of models and input of parameters. For the studies here we utilized the structural mechanics toolbox.

Using COMSOL Multiphysics poroelastic models have been examined against analytical solutions by Souley & Thoraval (2011). The software was applied for various fluid injection problems (Freeman *et al*., 2008), for CO_2 storage (Bjørnara *et al*. 2010) and for tight gas reservoirs (Hagemann et al. 2012). Spatafora & Boschetti (2010) study permeation tests. Rémond *et al*. (2008) as well as Nguyen *et al*. (2011) apply the software for a micro scale poroelastic problems.

We present benchmarks in spherical and in cylindrical geometry and compare with analytical solutions. Meshes are shown in Figure 1.

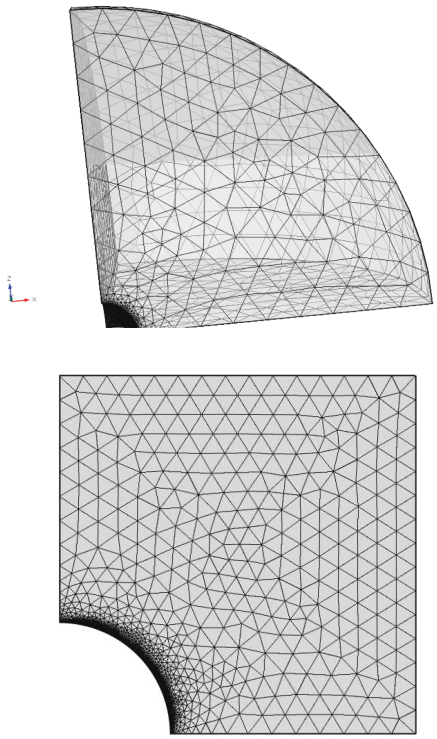

Figure 1. Benchmark model regions with meshes; for spherical cavity in 3D (top) and circular cavity in 2D (bottom)

Concerning flow a constant hydraulic gradient is assumed (in Figure 1 from right to the left). All other outer boundaries obey a no-flow condition, i.e. it is assumed that all boundaries are far enough away from the pumping regime on the vertical axis through the center of the model region in order to remain unchanged. The borehole is cut out of the permeable layers, and a mass flux condition is required at the so constructed inner surfaces, in order to achieve infiltration and pumping. In the baserock formation the borehole is not modeled, as the influence of the borehole on both hydraulic and mechanical regime in the large scale are surely not of importance. On the other hand meshing produces a significantly increased number of degrees of freedom of the numerical problem, if the borehole is considered entirely in the model geometry.

Concerning mechanics we allow free deformations in the interior and all boundaries, except the base at the bottom, where we require the spatial system to be fixed. Here we

present results for the steady state, as these represent the final maximum response of the geo-system to the changed constant stress regime.

Values for poroelastic parameters are adopted from various sources, as reported by Isaacs *et al*. (2008), Cappa (2009), Reyer and Philipp (2013). The elastic tensor is specified in our case by the Young modulus and the Poisson number. The reference parameters used in the model are gathered in Table 1. Most values were adopted from Grandhi *et al*. (2002).

Table 1. Reference Parameter Settings

Parameters			
Young modulus E [GPa]	52.0	Radius R [m]	0.311 (2D) 1.0 (3D)
Poisson ratio ν [-]	0.1486	Length L [m]	8.0 (2D) 10.0 (3D)
Permeability [m^2]	$1 \cdot 10^{-17}$	Vertical stress [GPa]	0.0644
Porosity [-]	0.08	Max. horizontal stress σ_H [GPa]	0.1481
Density [kg/m^3]	2422	Min. hor. stress / Max. hor. stress [-]	1.7/2.3
Biot parameter [-]	0.25		

4. Analytical Solutions

For the elastic problem of a circular hole in an infinite homogeneous model region and unidirectional stress a solution was first published by Kirsch (1898). For direction dependent maximum and minimum principal stresses σ_H and σ_h at the outer boundaries, the solution can be generalized to:

$$\sigma_\theta = \frac{1}{2}(\sigma_H + \sigma_h)\left(1+(R/r)^2\right) - \frac{1}{2}(\sigma_H - \sigma_h)\left(1+3(R/r)^4\right)\cos(2\theta) \quad (4)$$

(Jaeger & Cook, 1979).

The deformation **u** in radial coordinates for the unidirectional problem $\sigma_h = 0$ is given by

$$u_r = \frac{\sigma_H}{8\mu r}\left(r^2(\kappa+1)+R^2 + 2\left(R^2(\kappa+1)-\frac{R^4}{r^2}\right)\cos(2\theta)\right) \quad (5)$$

$$u_\theta = -\frac{\sigma_H}{4\mu r}\left(R^2(\kappa-1)+r^2+\frac{R^4}{r^2}\right)\sin(2\theta)$$

with $\kappa = 3-4\nu$ and shear stiffness $\mu = E/2(1+\nu)$ (Muskhelisvili 1953).

In the bi-axial tension case (p=p_0 at outer boundaries) for the 2D problem the solution is:

$$\sigma_r = p_0\left(1-(R/r)^2\right)$$
$$\sigma_\theta = p_0\left(1+(R/r)^2\right) \quad (6)$$

with radial velocity:

$$u_r = \frac{p_0}{4\mu r}\left(r^2(\kappa-1)+2R^2\right) \quad (7)$$

For the spherical cavity in a hydrostatic stress field, the analytical solution for the diagonal elements of the stress tensor are given by

$$\sigma_r = p_0\left(1-(R/r)^3\right)$$
$$\sigma_\theta = \sigma_\varphi = p_0\left(1+\tfrac{1}{2}(R/r)^3\right) \quad (8)$$

(Poulos & Davis, 1974) for Dirichlet boundary condition for pressure p=p_0 at the outer boundary. Off-diagonal terms vanish.

5. Results

For the circular cavity, modelled in 2D, Figure 2 shows the distribution of Tresca stress a result.

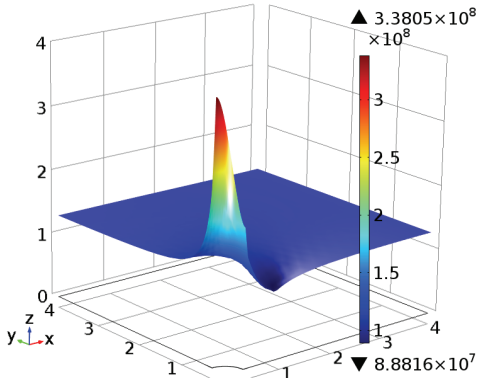

Figure 2: Tresca stress [Pa] of 2D reference problem in deformed mesh

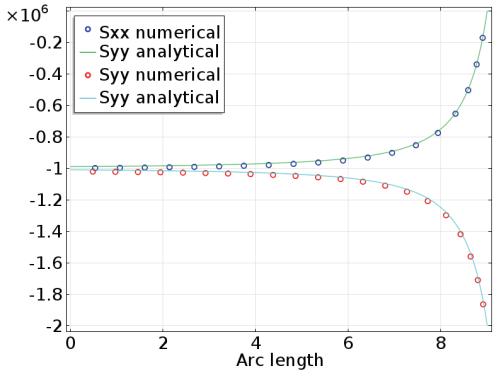

Figure 3: Stress tensor components in dependence of distance from inner radius for circular hole (2D); comparison with analytical solution (Length in [m], stresses in [Pa])

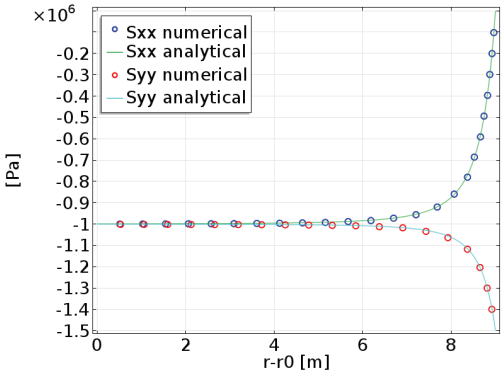

Figure 4: Stress tensor components in dependence of distance from inner radius for spherical hole (3D); comparison with analytical solution

A comparison between analytical and numerical results is depicted in Figure 3. The numerical model according to visual check performs quite well.

The spherical cavity, modelled in 3D, was modelled first in the solid mechanics mode. The comparison, depicted in Figure 4 also shows a good agreement between numerical and analytical results as in the 2D case.

A more detailed study of the error is based on the mesh refinements. Here we changed the mesh following the default mesh options in COMSOL Multiphysics, i.e. using the settings: extremely coarse, extra coarse, coarser, coarse, normal, fine, finer. The results are shown in Table 2. The corresponding execution times increased from 4 s for the extremely coarse mesh up to 62 s for the finer mesh.

Table 2: Mesh dependence of error for the spherical cavity benchmark

DOF	Max. error [Pa]	Convergence rate
31179	215300	
35541	35720	3.00
45867	24470	2.69
56691	18942	2.58
91317	16976	2.44
131874	9112	2.29
287544	7056	2.14

The maximum error is evaluated for the *x*-component of the stress tensor Sxx. The error decreases mesh refinement. The convergence rate is calculated following the derivations of Bradji & Holzbecher (2007, 2008). Thus we find a convergence rate decreasing from a value of 3 for coarse mesh refinements down to 2 for the fine meshes.

As a first parameter study for the 2D problem we first investigated the influence of the model extension. The analytical solutions, given above are valid for a set-up with infinite length.

Figure 5 depicts the angular stress along the hole boundary (0-90°) for lengths, as indicated by the length value in the legend (in [m]). The highest deviation from the analytical solution is for the smallest model, and with increasing model length the numerical results converge against the analytical solution. For further parameter studies we decided that length L=8 is a sufficient and appropriate value.

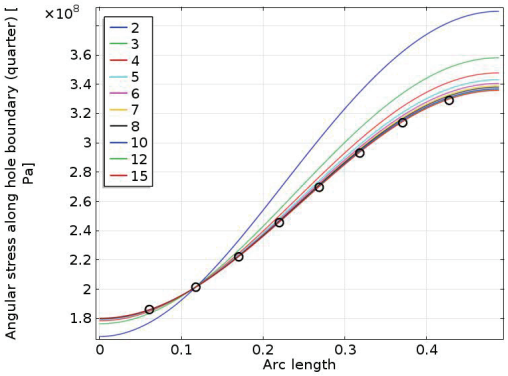

Figure 5: Angular stress along hole boundary in dependence of model extension (in [m])

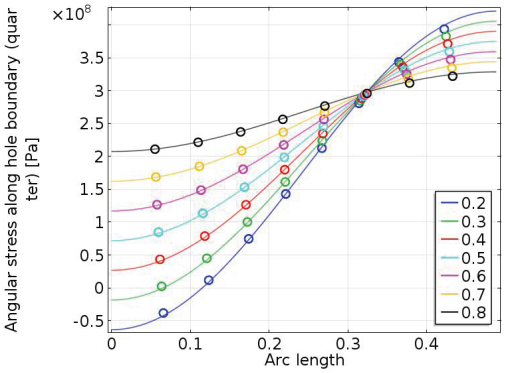

Figure 6: Angular stress along hole boundary in dependence of stress contrast at outer boundaries

As next step we examine the influence of the stress contrast (σ_h / σ_H) on the performance of the numerical models. Figure 6 depicts the results. The analytical solutions are indicated by circle markers, while the lines represent the outcome of the numerical simulations.

Obviously the numerical model performs well. It can be seen that for low contrasts the angular stress component changes its sign, i.e. it changes between tensional and pressurized regimes (compare: Grandhi et al. 2002).

Concerning accuracy it turns out that deviation between analytical and numerical solutions is higher for lower contrasts.

For k=0 we therefore checked the accuracy in more detail. Figure 7 shows the mesh dependency for that case, calculated for L=8. An initial mesh with 658 triangular elements (refined at the hole boundary) was refined four times. The figure shows the radial stress along the hole boundary, as modelled. The value corresponds with the model error, as the radial stress is zero for the modelled situation, and thus indicates the performance.

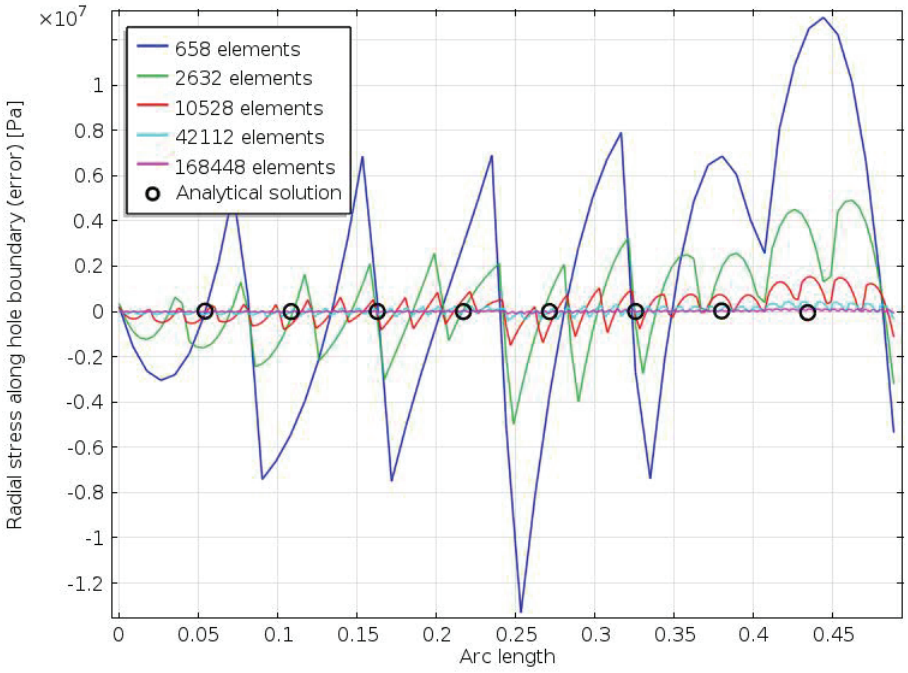

Figure 7: Radial stress error along hole boundary in dependence of grid refinement

For this variable we examined the mesh dependence of the error. For a wider model region L=64 the convergence rates were checked, following the work outlined by Bradji & Holzbecher (2007, 2008). For the error of angular stress in the max. norm for successive mesh refinement we observe a convergence to the limit convergence rate of 2 from below. Details are given in Table 3.

Table 3: Error evaluation for the 2 benchmark

DOF	Max. error [Pa]	Convergence rate
3592	1.6843e7	
13949	6.0152e6	1.5179
54967	1.9848e6	1.6171
218219	6.1165e5	1.7075
869587	1.6777e5	1.8713
3471779	45316	1.8910

In contrast to the former mesh dependence study the mesh refinement was performed manually. The DOF (degrees of freedom) thus roughly increases by a factor of four from one mesh to the other. Thus the mesh sequence is a much better choice for the determination of the convergence rate, than using the predefined meshes as used before for the 3D cavity. Thus we see observe an increase of the convergence rate up to 2.

For $\sigma_h = 0$ we examined the deformation itself also. Figure 8 depicts the numerical values and analytical solutions. For radial as well as for angular deformations, numerical and analytical solutions coincide well.

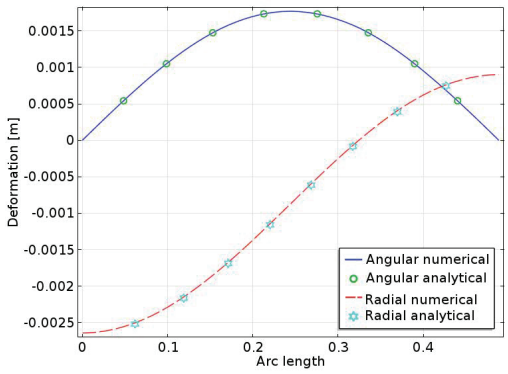

Figure 8: Deformation in elastic uni-axial stress problem

6. Conclusions

Cavity models have been examined in two and three dimensions. Comparisons with analytical solutions show that the finite element models, set up using COMSOL Multiphysics, perform well.

With increasing mesh refinement the convergence rate for the 2D model becomes almost quadratic for the 2D cavity. For the 3D cavity it is almost cubic for coarse meshes. However, using the mesh refinements, predefined in COMSOL Multiphysics, the convergence rate decreases to almost quadratic.

References

1. Biot, M.A., General theory of three-dimensional consolidation, *J. of Applied Physics* **12**, 155-164 (1941)
2. Bjørnara T.J., Aker E., Cuisiat F., Skurtveit E., Modeling CO_2 storage using coupled reservoir-geomechanical analysis, *COMSOL Conf.*, Paris, Proceedings (2010)
3. Bradji A., Holzbecher E., On the convergence order of COMSOL solutions, COMSOL Conf., Grenoble (2007)
4. Bradji A., Holzbecher E., On the Convergence Order in Sobolev Norms of COMSOL Solutions, COMSOL Conf., Budapest (2008)
5. Cappa, F., Modelling fluid transfer and slip in a fault zone when integrating heterogeneous hydromechanical characteristics in its internal structure, *Geophys. J. Int.* **178,** 1357–1362 (2009)
6. Carcione J.M., Morency C., Santos J.E., Computational poroelasticity – a review, *Geophys*. **75**(5), 75A229-75A243 (2010)
7. Cowin S.C., Doty S.B., Tissue Mechanics, Springer, New York (2007)
8. Freeman T.T., Chalaturnyk R.J., Bogdanov I.I., Fully coupled thermo-hydro-mechanical modeling by COMSOL Multiphysics, with applications in reservoir geomechanical characterization, *COMSOL Conf.*, Boston, Proceedings (2008)
9. Grandi S., Rao R., Nafi Toksöz M., Geomechanical modeling of in-situ stresses around a borehole, MIT lab reports (http://erl.mit.edu/lab-reports.php) (2002)
10. Hagemann B., Wegner J., Ganzer L., Investigation of hydraulic fracture re-orientation

effects in tight gas reservoirs, *COMSOL Conf*., Milan, Proceedings (2012)
11. Isaacs A.J., Evans J.J., Kolesar P.T., Nohara T., Composition, microstructures, and petrophysics of the Mozumi fault, Japan: In situ analyses of fault zone properties and structure in sedimentary rocks from shallow crustal levels, *J. Geophys. Res*. **113**, B12408, doi:10.1029/2007JB005314 (2008)
12. Jaeger J.C., Cook N.G., *Fundamentals of Rock Mechanics*, Chapman and Hall, London (1979)
13. Kirsch, G. (1898). Die Theorie der Elastizitat und die Bedürfnisse der Festigkeitslehre. *Veit. Deit. Ing.* 42 (28), 797-807.
14. Morency C., Huismans R.S., Beaumont C., Fullsack P., A numerical model for coupled fluid flow and matrix deformation with applications to disequilibrium compaction and delta stability, *J. Geophys. Res*.**112**, B10407 (2007)
15. Muskhelishvili, N.I., *Some Basic Problems of the Mathematical Theory of Elasticity*, Noordhoff, Groningen (1953)
16. Nguyen V.-H., Lemaire T., Naili S., Influence of interstitial bone microcracks on strain-induced fluid flow, *Biomech. Model Mechanobiol*. **10**, 963-972 (2011)
17. Poulos H.G., Davis E.H., Elastic Solutions for Soil and Rock Mechanics, Wiley, New York (1974)
18. Rémond A., Naili S., Lemaire, T., Interstitial fluid flow in the osteon with spatial gradients of mechanical properties: a finite element study, *Biomech. Model Mechanobiol*. **7**, 487-495 (2008)
19. Reyer D., Phillip S.L., Correlations of rock mechanical and physical properties with uniaxial compressive strengths of sedimentary rocks from the Northwest German Basin, to appear (2013)
20. Souley M., Thoraval A., Nonlinear mechanical and poromechanical analyses: comparison with analytical solutions, *COMSOL Conf*., Stuttgart, Proceedings (2011)
21. Spatafora G., Boschetti, F., Finite element analysis of permeation tests on articular cartilage under different testing conditions using COMSOL Multiphysics, *COMSOL Conf*., Paris, Proceedings (2010)

Acknowledgement

The author appreciates the support of 'Niedersächsisches Ministerium für Wissenschaft und Kultur' and ‘Baker Hughes’ within the GeBo G7 project.